Solar source of the largest geomagnetic storm of cycle 23

N. Gopalswamy[1], S. Yashiro[1,2], G. Michalek, H. Xie[1,2], R. P. Lepping[1], and R. A. Howard[3]

[1]NASA Goddard Space Flight Center, Greenbelt, MD, USA

[2]The Catholic University of America, Washington, DC, USA

[3]Naval Research Laboratory, DC, USA

The largest geomagnetic storm of solar cycle 23 occurred on 2003 November 20 with a Dst index of -472 nT, due to a coronal mass ejection (CME) from active region 0501. The CME near the Sun had a sky-plane speed of ~1660 km/s, but the associated magnetic cloud (MC) arrived with a speed of only 730 km/s. The MC at 1 AU (ACE Observations) had a high magnetic field (~56 nT) and high inclination to the ecliptic plane. The southward component of the MC's magnetic field was made up almost entirely of its axial field because of its east-south-west (ESW) chirality. We suggest that the southward pointing strong axial field of the MC reconnected with Earth's front-side magnetic field, resulting in the largest storm of the solar cycle 23.

1. Introduction

Large geomagnetic storms (Dst < -100 nT) are generally caused by Earth-directed coronal mass ejections (CMEs) that evolve into interplanetary CMEs (ICMEs). Only moderate to weak storms are caused by high speed streams from coronal holes (see, e. g., Sheeley et al., 1976). Although the close association between CMEs and magnetic storms has been established sometime ago (Wilson, 1987; Gosling, et al. 1990), we are far from being able to quantitatively relate Earth-directed CMEs and geomagnetic storms. The main reason is the lack of information on the interplanetary evolution of CMEs due to their coupling with the variable ambient flow (Gonzalez et al., 1999; Lepping et al., 2003). We illustrate this complex problem using the 2003 November 20 storm, which was the largest in the current solar cycle 23 (as of this writing), traced to a CME that erupted on November 18. This is a case study attempting to understand the circumstances under which such an extreme storm could occur.

2. The Geomagnetic Storm and the Magnetic Cloud

Figure 1 shows a plot of the Dst index obtained from the World Data Center in Kyoto (http://swdcdb.kyoto-u.ac.jp/dstdir/dst1/prov.html). The storm started with the arrival of the shock at 07:28 UT on November 23 and reached a minimum Dst value of -472 nT at 20:00 UT followed by an extended recovery phase. The storm started rapidly intensifying with the arrival of an ICME at ~10:00 UT. The ICME was a magnetic cloud (MC) and was driving a shock, which was detected at L1 around 07:28 UT by the proton monitor on board the Solar and Heliospheric Observatory (SOHO) mission. The plasma and

magnetic observations from the Advanced Composition Explorer (ACE) revealed that the MC was an east-south-west (ESW) cloud with its axis nearly perpendicular to the ecliptic (Fig. 1). The axial field was pointing south for the duration (~13.5 h) of the cloud with a maximum strength of ~56 nT. Static force-free flux-rope fitting (Lepping et al., 1990) showed that the inclination was ~73.4^{o} with an axial field strength of 46.5 nT and a flux of 1.3x10^{21} Mx. The MC was expanding, evidenced by the smooth decrease in speed from the front (738 km/s) to the back (531 km/s). The average cloud speed was ~635 km/s. The proton plasma beta was low (<<1) and the density was highly variable inside the MC. The profile of the total magnetic field was also structured with a sharp drop from the peak followed by a slower decrease. The MC was followed by a moderate speed stream with a speed of ~600 km/s and a density exceeding 15 cm^{-3}. The average cloud speed and the stream speed were nearly the same, but considerably higher than the upstream speed (450 km/s).

The geomagnetic storm and the responsible MC were extreme events in their respective classes. This is illustrated in Figure 2 with the distributions of intensities of all storms of solar cycle 23 with Dst < -100 nT and the maximum values of the field strengths (Bmax) of all the observed MCs (1994 to the end of 2003). Most of the MCs were obtained from the Wind Magnetic Filed Investigation (MFI) site (http://lepmfi.gsfc.nasa.gov/mfi/mag_cloud_pub1.html); ACE data were used when Wind was not in the solar wind. Clearly the 2003 November 20 event is the sole member of the largest bins in both the distributions. Note that all the three storms from the 2003

October- November period belong to the top five in both the distributions. There was only one other super storm (March 13, 1989) in the space age with a higher Dst (-589 nT).

The Dst and Bmax ordering is not quite the same, because the Dst index is decided by additional factors such as the strength of the southward component and the speed of the MCs. The smallest of the five MC events in the Bmax distribution (2000 August 12 MC) does not show up in the Dst top five, because the corresponding Dst was only -235 nT (still an intense storm). The intense storm on 2001 March 31 (Dst = -387 nT) does not show up in the top five of the Bmax distribution, because the ICME could not be fit to a cloud. However, the magnetic field strength of the ICME was high (39 nT) and contained intervals of southward field. Gonzalez et al. (1998) obtained the following relation between peak MC field strength (B) and speed (V) of MCs: B (nT) = 0.047V (km/s) -1.1. If we substitute V= 730 km/s for the November 20 MC, we get B = 33.2 nT, which is much smaller than the observed 56 nT (~70% higher than predicted), suggesting that this MC is unusual. There were other clouds with similar speeds in agreement with Gonzalez et al. (1998) result, but the associated storms were less intense (-311 nT) (Tsurutani et al., 1992).

3. The Solar Source

3.1 Identification of the Solar Source

The only prominent source region on the solar disk was active region (AR) 501, which was the return of AR10484 – one of the three active regions that caused a large number of X-class flares and fast coronal CMEs during the previous rotation. AR501 appeared on

the east limb on November 13 and produced several M-class flares and a large number of C and B-class flares during its disk passage. Since the solar sources of MCs are typically located within $\pm 30^{o}$ from the disk center (see, e.g., Gopalswamy et al. 2000b), we looked for eruptions in this longitude range 1-3 days before the shock arrival at Earth (2003 November 20 at 07:23 UT) using SOHO's Large Angle and Spectrometric Coronagraph (LASCO) data. We also searched for EUV eruption signatures using SOHO's Extreme-ultraviolet Imaging Telescope (EIT) data to confirm that the CMEs originated from the active region in question. Movies of superposed EIT and LASCO images showed that there were no CMEs from AR501 during November 14-16. There were only B and C-class flares during these days. There were two M-class flares on 2003 November 17: an impulsive flare at 01:28 UT that did not have a detectable CME and a large CME heading to the southeast with an average speed of ~1061 km/s. The CME consisted of a bright core and a faint extended region and the direction of motion was consistent with the location of AR 501 at S01E33. On November 18, there were two CMEs from AR501, one at 08:06 UT (speed ~ 1223 km/s; width ~ 104^{o}) and the other at 08:50 UT (speed ~ 1660 km/s; halo). The active region was in the right longitude range at N00E18 so that the CME was likely to arrive at 1 AU. Since the CME on November 17 was confined mostly to the southeast with minimal overlap with Earth direction, we associate the November 20 MC with the 08:50 UT CME on November 18. Other CMEs on November 19 were too slow to be associated with the MC in question. There was also a very fast CME (1834 km/s) on November 18 at 09:50 UT, but it was from the east limb and hence was not likely to arrive at Earth.

The three CMEs (labeled CME1, CME2, and CME3) of November 18 are shown in Figure 3 along with their height-time plots and the GOES soft X-ray light curve in the 1-8 Å channel. Each of the three CMEs was associated with an M-class flare as indicated on the light curve. The flare associated with CME3 was partly behind the east. CME1 was mostly confined to the southeast. CME2 had a very bright inner structure with its apex in the southwest direction moving with a speed of 1633 km/s. The eastern flank of CME2 was moving with a speed of 1229 km/s in the direction of CME1. It is highly likely that the propagation of CME2 was influenced by the preceding CME1 and the neighboring CME3. Since the November 20 MC is the evolved form of CME2, we note that it has undergone severe deceleration from 1660 km/s near the Sun to 738 km/s at Earth. This amounts to a deceleration of 5.2 ms^{-2}, which is not too different from what is expected from the linear relationship between the acceleration (a) and CME speed (V) near the Sun (see, Gopalswamy et al., 2001): a (ms^{-2}) = 2.193 – 0.0054V (km/s). For V = 1660 km/s, this relation gives a deceleration of 6.8 ms^{-2}.

3.2 Near-surface Activities

Details of the source region as obtained from an H-alpha picture, a series of EIT images and a longitudinal magnetogram of from SOHO's Michelson Doppler Imager (MDI) are shown in Fig. 4. A thick U-shaped filament was located in the active region, with its apex pointing in the southwest direction (Fig.4a). A trace of the outer edge of the H-alpha filament is superposed on all the images for reference. The axis of the filament seems to trace the curved neutral line connecting the positive polarity in the north to the negative polarity in the south (Fig. 4b). The north-south segment of the filament was significantly

larger than the east-west segment. The filament with filament channel appeared as a thick dark feature in the EUV images (see Fig. 4c). Eruption of this filament resulted in a bright post-eruption arcade overlying the pre-eruption position of the east-west segment of the filament (Fig. 4e), but the EUV ribbon can be seen along entire filament at 08:12 UT (Fig. 4d). Fragments of the filament near the southern leg seem to have erupted during two previous flares from AR501, but the entire filament erupted during CME2. The online Solar Geophysical Data reported the location of the filament disappearance from S04E16, as is also clear from Fig. 4. One can associate the inner part of CME2 with the erupted filament, because the morphology and direction of the two features is similar (see Fig. 3). The presence of the large coronal hole to the east and north of the eruption region might have constrained the motion of the CME to the southwest. Similar constraining of CME motion by Sun's global dipolar field and polar coronal holes have been reported before (Gopalswamy et al., 2000a; 2003). A low-latitude coronal hole had similarly constrained a disk center CME (2000 August 9 at 10:30 UT) to the western hemisphere (Gopalswamy et al., 2004). We must point out that the filament was located to the southwest of AR501, so one cannot rule out the possibility that the structure of the active region itself might have caused such a trajectory for the filament.

4. Why the Superstorm?

Although the speed of the CME was not extreme compared to the events from AR 486, the November 20 MC was remarkable in two respects: (1) the MC axis had a high inclination to the ecliptic plane with the axial field pointing southward, and (2) the magnitude of the magnetic field was the largest of the solar cycle. The important

consequence of the strongly tilted ESW MC was that its Bz was almost entirely due to the strong axial field, and hence very geoeffective (see e.g., Gonzalez et al., 1994). The axial field of the MC was nearly anti-parallel to Earth's front-side magnetic field, leading to sustained reconnection and, hence, the intense geomagnetic storm. Although the photospheric neutral line was curved, the north-south segment was the largest, consistent with the high inclination (-73^{o}) of the MC axis. The bright post-eruption arcade at the location of the east-west segment of the filament suggests the possibility that this segment was propelled faster, thus contributing to the predominant north-south orientation of the erupted filament. The axes of interplanetary flux ropes are typically aligned with the neutral line at the Sun (see e.g., Mulligan et al. 1998). The November 20 MC seems to be consistent with this pattern because of the large north-south extent of the filament. However, we do not think that the filament itself became the MC. The flux rope is likely to be a larger structure enclosing the filament. The magnetic field direction (southward) in the filament is also consistent with the direction of the axial field of the MC.

The extreme field strength of the MC may be due to a combination of factors: (1) the flux rope originated in an active region, so it is expected to have a higher field strength compared to one from quiescent filament regions, and (2) the difference between the MC speed and the upstream speed was relatively large, so the MC would have suffered a strong front-side compression, consistent with the observed profile in Fig. 1. Additional possibilities are: (1) the high speed stream from the coronal hole might have compressed

the cloud to some extent, and (2) the CME interacted with another CME from the same region that departed an hour earlier and might have contributed to some compression.

A fully-southward, high inclination (-80^o) MC was observed on 1978 August 27 by IMP-8 and ISEE 3 spacecraft (Burlaga 1988). We found that this MC had resulted in an intense storm (Dst = -226 nT) that lasted for a few days. The maximum field strength of this MC was only 23 nT compared to the 56 nT for the November 20 MC, explaining the smaller Dst index. The speed (~ 460 km/s) was also relatively low (Lepping et al., 1990). Another fully-southward, high inclination (-64^o) MC that occurred during 1978 October 29-November 1 was reported by Lepping et al. (2003). The associated storm had a Dst of ~ -88 nT, because the axial field strength was only 14 nT. The opposite case of MCs with no associated geomagnetic storm happens when the MCs have high inclination and northward axial field. The 1971 June 21 MC with an axial field of ~11 nT (see Burlaga, 1988) had no geomagnetic storm at all because it was a high inclination (60^o), fully-northward cloud. The 2000 February 21 MC is another example with no storm at all (Yurchyshyn et al. 2001).

5. Discussion and Conclusions

We have shown that the largest geomagnetic storm of solar cycle 23 was caused by a fast and wide CME originating from close to disk center that resulted in a highly inclined MC with its axial field pointing almost always southward. In addition, the axial field was unusually strong and the speed of the MC was well above average. Since the axial field strength is typically larger than of the azimuthal field strength near its boundary, a very

strong southward field must have interacted with Earth's magnetic field. It is important to identify and study such fully-southward MCs, because they do not have a specific pattern with respect to the solar cycle (Mulligan et al. 2001) and hence it is hard to predict their occurrence. The 2003 November 20 superstorm thus makes the highly inclined MC with southward field a new addition to the list of interplanetary conditions that may lead to a superstorm (Gonzalez et al., 1999). This event also brings out the importance of other events such as coronal holes and CMEs that occur in spatial and temporal proximity to the storm-causing CME event.

Acknowledgments: We thank N. Ness for ACE data and T. Narock for help with Figure 1. We thank the referees for their helpful comments. This research was supported by NASA LWS and NSF SHINE (ATM 0204588) programs. SOHO is a project of international cooperation between ESA and NASA.

References

Burlaga, L. Magnetic Clouds: Constant-alpha force free configurations, J. Geophys. Res., 93, 7217, 1988

Gopalswamy, N., Y. Hanaoka, and H. S. Hudson, Structure and Dynamics of the corona surrounding an eruptive prominence, Adv. Space Res., 25, No.9, 1851, 2000a

Gopalswamy, N. ., A. Lara, R. P. Lepping, M. L. Kaiser, D. Berdichevsky, and O. C. St. Cyr, Interplanetary acceleration of coronal mass ejections, Geophys. Res. Lett. Vol. 27, No. 2, p. 145, 2000b.

Gopalswamy, N., A. Lara, S. Yashiro, M. L. Kaiser, and R. A. Howard, Predicting the 1-AU arrival times of coronal mass ejections, J. Geophys. Res., 106, 29207, 2001

Gopalswamy, N., M. Shimojo, W. Lu, S. Yashiro, K. Shibasaki, and R. A. Howard, Prominence eruptions and coronal mass ejections: A statistical study using microwave observations, Astrophys. J., 586, 562, 2003

Gopalswamy, N., S. Yashiro, S. Krucker, G. Stenborg, and R. A. Howard, Intensity variation of large solar energetic particle events associated with coronal mass ejections, J. Geophys. Res., in press, 2004

Gonzalez, W. D., J. A. Joselyn, Y. Kamide, H. W. Kroehl, G. Rostoker, B. T. Tsurutani, and V. M. Vasyliunas, J. Geophys. Res., 99, 5771, 1994

Gonzalez, W. D., C. de Gonzalez, A. Dal Lago, B. T. Tsurutani, J. K. Arballo, G. S. Lakhina, B. Buti, C. M. Ho, and S. T. Wu, Geophys. Res. Lett., 25, 963, 2001

Gonzalez, W., B. T. Tsurutani, and A. L. C. de Gonzalez, Interplanetary origin of geomagnetic storms, Space Sci. Rev., 88, 529, 1999

Gosling, J. T., S. J. Bame, D. J., McComas, and J.L. Phillips, Coronal mass ejections and large geomagnetic storms, Geophys. Res. Lett., 127, 901, 1990

Lepping, R. P., J. A. Jones and L. F. Burlaga, Magnetic field structure of interplanetary magnetic clouds at 1 AU, J. Geophys. Res., 95, 11957, 1990

Lepping, R. P., D. Berdichevsky, and C. C. Wu, Sun-Earth electrodynamics: The solar wind connection, Research Signpost, 37/661 (2), 151, 2003

Mulligan, T., C. T. Russell, and J. G. Luhmann, Solar cycle evolution of the structure of magnetic clouds in the inner heliosphere, Geophys. Res. Lett., 25, 2959, 1998

Mulligan, T., C. T. Russell, D. Elliott, J. T. Gosling, and J. G. Luhmann, Inversion studies of magnetic cloud structure at 0. 7 AU: Solar cycle variation, Geophys. Res. Lett., 28, 891, 2001

Sheeley, N. R. Jr., J. W. Harvey, and W. C. Feldman, Coronal holes, solar wind streams, and recurrent geomagnetic disturbances, 1973-1976, Sol. Phys., 49, 271, 1976

Tsurutani, B. T., W. D. Gonzalez, F. Tang, and Y. T. Lee, Great magnetic storms, Geophys. Res. Lett., 19, 73, 1992.

Wilson, R. M., Geomagnetic response to magnetic clouds, Planet. Space Sci., 35, 329, 1987

Yurchyshyn, V., Wang, H., P. R. Goode, and Y. Deng, Orientation of the magnetic fields in interplanetary flux ropes and solar filaments, Astrophys. J., 563, 381, 2001

Figure Captions

Figure 1. The 2003 November 20 geomagnetic storm index (Dst), the magnetic field strength (|B|), the latitude (θ_B), longitude (φ_B) of the associated magnetic cloud (MC), and the solar wind parameters (proton density N_p, thermal speed V_{th}, flow speed V and the plasma beta β). The dashed curves in the |B|, θ_B, and φ_B panels represent the model fits. The boundaries of the cloud (MC) and the shock (S) are marked at the top.

Figure 2 (a) Distribution of the intensity (determined by Dst $\leq$ -100 nT) of 67 distinct cycle 23 storms (1996-2003). (b) Distribution of the maximum observed field strength (Bmax) of all the identified 85 magnetic clouds since the launch of Wind in November 1994 until the end of 2003. The top five events in each distribution are marked

(YYMMDD format). The 2003 November 20 event is the topmost in both the distributions.

Figure 3. SOHO/LASCO images (top) showing the three white-light CMEs of interest, along with their height-time plots (middle) and the GOES X-ray light curve (1-8 A) with flares marked (bottom). CME1 and CME2 originated from AR501, while CME3 originated from the east limb. The inner structure of CME2 is also shown, which seems to be related to the filament eruption from AR501.

Figure 4. (a) H-alpha picture from the Mauna Loa Solar Observatory showing the U-shaped dark filament taken before the eruption. (b) SOHO/MDI magnetogram showing the line-of-sight magnetic field structure of the active region (white: positive polarity; black – negative polarity). A trace of the outer edge of the H-alpha filament is superposed on the magnetogram. (c) SOHO/EIT image with superposed contours of line-of-sight magnetic field (red: positive or north; blue – negative or south). The trace of the H-alpha filament outlines the outer edge of the EUV filament (or filament channel). (d) SOHO/EIT image showing the ribbon structure due to the eruption of the entire filament. (e) Post-eruption arcade around the location of the southern leg (east-west segment) of the filament.

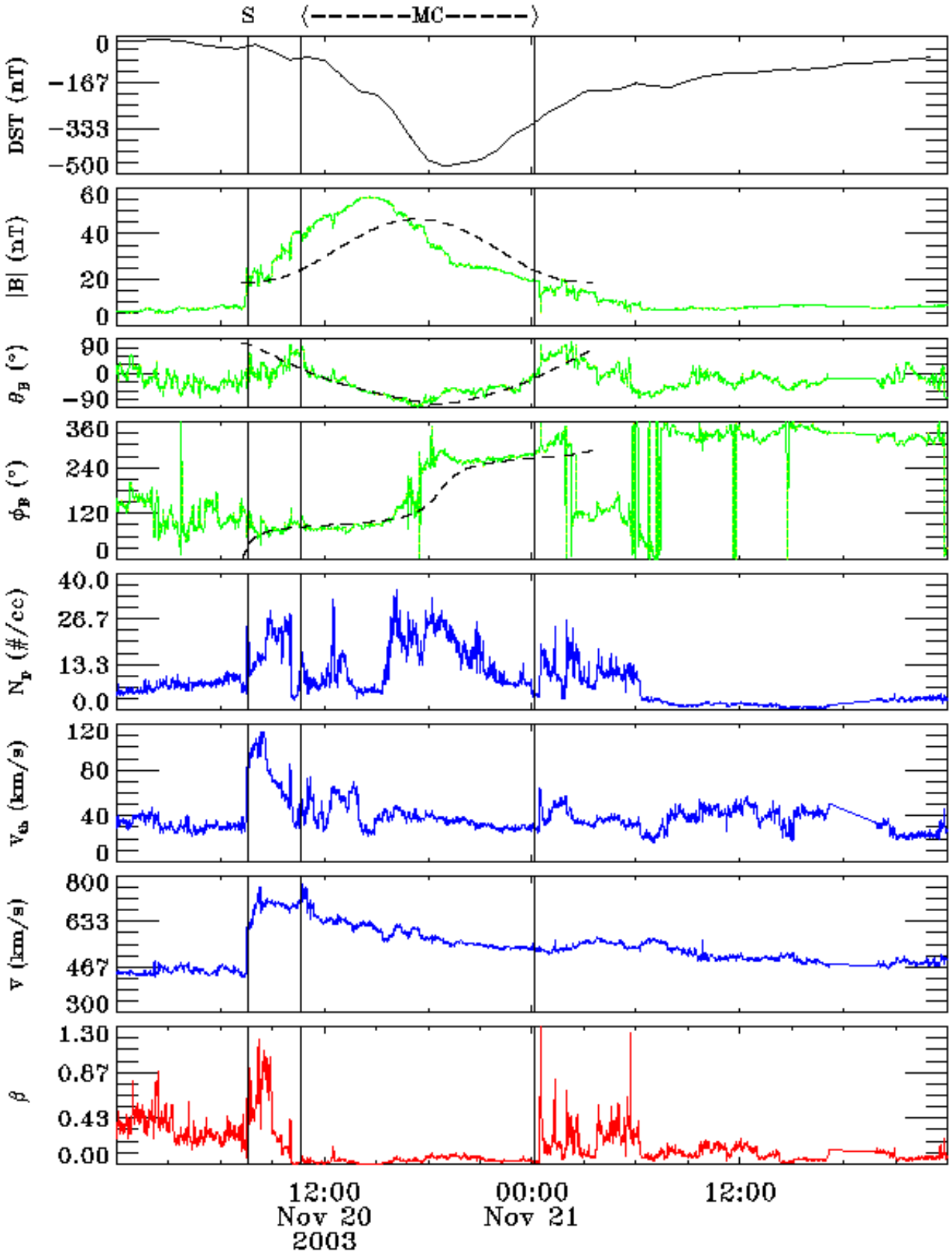
S
⟨------MC------⟩
DST (nT)
0
−167
−333
−500
|B| (nT)
60
40
20
0
θB (°)
90
0
−90
φB (°)
360
240
120
0
Np (#/cc)
40.0
26.7
13.3
0.0
Vsw (km/s)
120
80
40
0
v (km/s)
800
633
467
300
β
1.30
0.87
0.43
0.00
12:00
Nov 20
2003
00:00
Nov 21
12:00

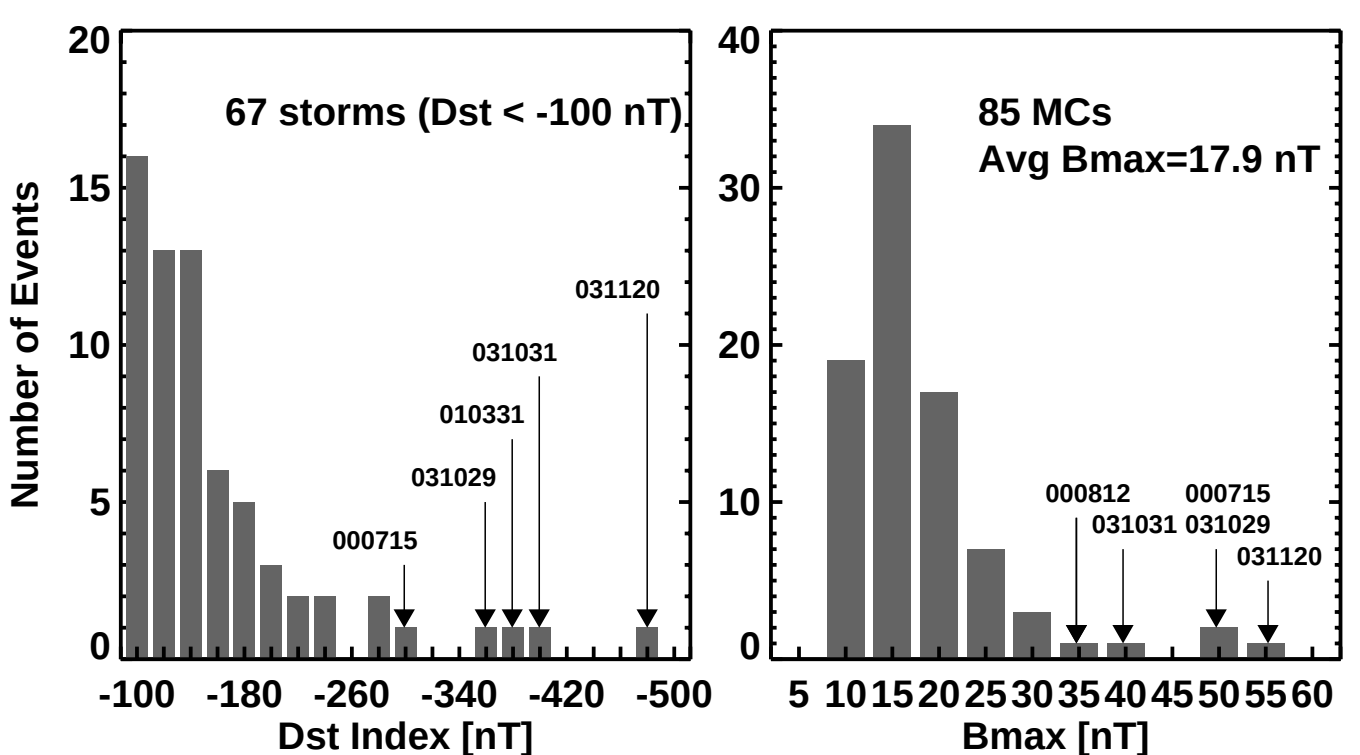
67 storms (Dst < -100 nT)
Number of Events
Dst Index [nT]
-100
-180
-260
-340
-420
-500
000715
031029
010331
031031
031120
85 MCs
Avg Bmax=17.9 nT
Bmax [nT]
000812
031031
000715
031029
031120

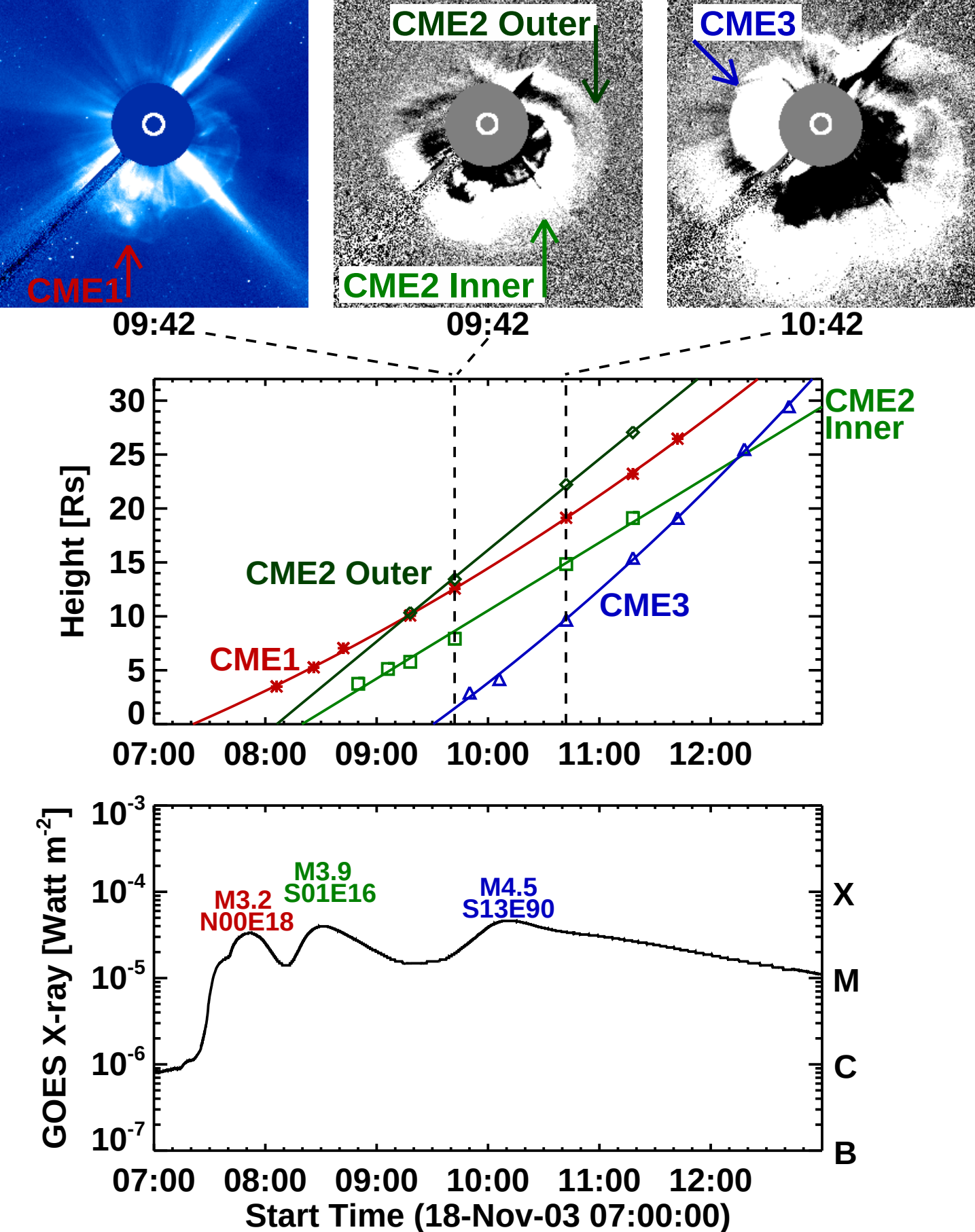
CME1
CME2 Outer
CME2 Inner
CME3
09:42
09:42
10:42
Height [Rs]
30
25
20
15
10
5
0
CME2 Outer
CME1
CME3
CME2 Inner
07:00
08:00
09:00
10:00
11:00
12:00
GOES X-ray [Watt m-2]
10-3
10-4
10-5
10-6
10-7
M3.2
N00E18
M3.9
S01E16
M4.5
S13E90
X
M
C
B
07:00
08:00
09:00
10:00
11:00
12:00
Start Time (18-Nov-03 07:00:00)

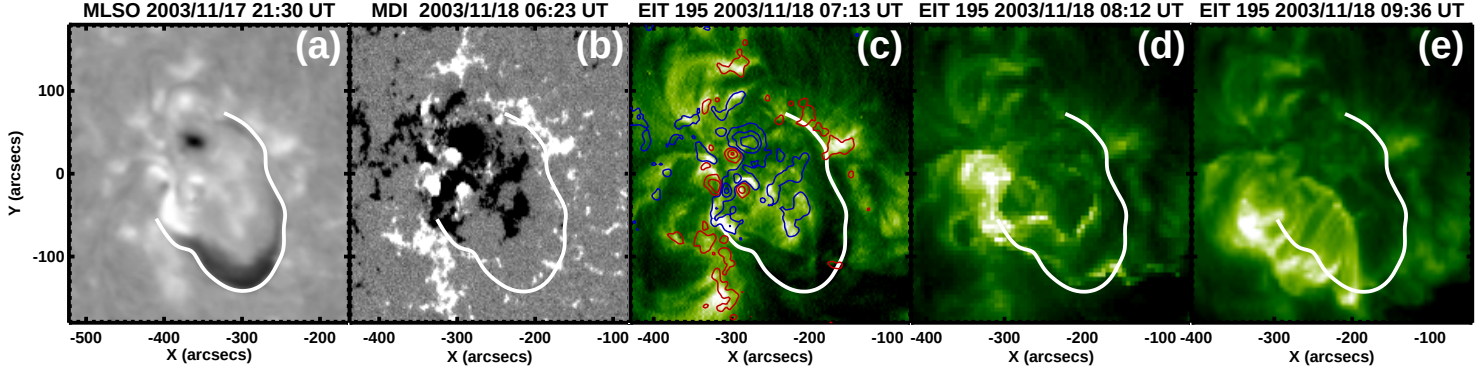
MLSO 2003/11/17 21:30 UT
MDI 2003/11/18 06:23 UT
EIT 195 2003/11/18 07:13 UT
EIT 195 2003/11/18 08:12 UT
EIT 195 2003/11/18 09:36 UT
(a)
(b)
(c)
(d)
(e)
Y (arcsecs)
100
0
-100
-500
-400
-300
-200
-100
X (arcsecs)